

# Finite element analysis and axial bearing capacity of steel reinforced recycled concrete filled square steel tube columns

Jing Dong<sup>1</sup>, Hui Ma<sup>\*1,2</sup>, Changming Zou<sup>1</sup>, Yunhe Liu<sup>1,2</sup> and Chen Huang<sup>1</sup>

<sup>1</sup>School of Civil Engineering and Architecture, Xi'an University of Technology, Xi'an, 710048, China

<sup>2</sup>State Key Laboratory of Eco-hydraulic Engineering in Arid Area, Xi'an University of Technology, Xi'an, 710048, China

(Received March 8, 2019, Revised May 6, 2019, Accepted May 7, 2019)

**Abstract.** This paper presents a finite element model which can simulate the axial compression behavior of steel reinforced recycled concrete (SRRC) filled square steel tube columns using the ABAQUS software. The analytical model was established by selecting the reasonable nonlinear analysis theory and the constitutive relationship of material in the columns. The nonlinear analysis of failure modes, deformation characteristics, stress nephogram, and load-strain curves of columns under axial loads was performed in detail. Meanwhile, the influences of recycled coarse aggregate (RCA) replacement percentage, profile steel ratio, width thickness ratio of square steel tube, RAC strength and slenderness ratio on the axial compression behavior of columns were also analyzed carefully. It shows that the results of finite element analysis are in good agreement with the experimental results, which verifies the validity of the analytical model. The axial bearing capacity of columns decreased with the increase of RCA replacement percentage. While the increase of wall thickness of square steel tube, profile steel ratio and RAC strength were all beneficial to improve the bearing capacity of columns. Additionally, the parameter analysis of finite element analysis on the columns was also carried out by using the above numerical model. In general, the SRRC filled square steel tube columns have high bearing capacity and good deformation ability. On the basis of the above analysis, a modified formula based on the American ANSI/AISC 360-10 was proposed to calculate the nominal axial bearing capacity of the columns under axial loads. The research conclusions can provide some references for the engineering application of this kind of columns.

**Keywords:** recycled aggregate concrete; steel reinforced recycled concrete; square steel tube column; axial compression behavior; finite element analysis

## 1. Introduction

Natural concrete aggregates and other non-renewable resources have been over-exploited. Furthermore, the demolition of abandoned buildings also produced a large amount of the construction waste, which had brought an unfavorable influence on the natural environment. Therefore, how to deal with the construction waste (Attaullah *et al.* 2013, Rachid *et al.* 2018 and Caglar *et al.* 2019) and reduce the exploitation of non-renewable resources has become one of the urgent problems to be solved in the world. Recycled aggregate concrete (RAC) (Zhang *et al.* 2018, Lais *et al.* 2017, Rafaela *et al.* 2016, Poon *et al.* 2002, Sepani *et al.* 2017, Rupyru *et al.* 2015, Kaznhisa *et al.* 2014, Howji *et al.* 2003, Lai *et al.* 2016), where the waste concrete is used as recycled coarse aggregate (RCA) instead of natural aggregate partly or completely, is a kind of green construction material. It has made effective use of waste concrete and caused a positive contribution to the sustainable development of construction industry. Therefore, the application of RAC material is very beneficial to the ecological environment protection. So far,

the researches on the basic mechanical properties of RAC material were carried out by many domestic and foreign scholars (Montero *et al.* 2017, Zhou and Chen 2017, Thamas. *et al.* 2013, Xiao *et al.* 2012, Papayianni 2003, Saroj *et al.* 2002). The main research contents of RAC material include the strength, deformation, elastic modulus, shrinkage, durability, fatigue property, constitutive relation and so on. A large number of research results show that the basic mechanical properties of RAC material are generally inferior to those of ordinary concrete due to the defects of RCA, which limits the engineering application of RAC material to a large extent.

Steel columns have high bearing capacity, but they are prone local buckling under various working conditions (Young 2005, Li *et al.* 2009, Rami *et al.* 2012). Steel and concrete composite structures, such as steel reinforced concrete structure, concrete filled steel tube structure, which effectively combine the advantages of concrete and steel structures, are widely used in high-rise buildings and bridge structures in recent years. Accordingly, some scholars adopted RAC materials in steel and concrete composite structures (Tang *et al.* 2018, Xiao *et al.* 2011, Lin *et al.* 2015, Ma *et al.* 2016, Yang 2015, Chen *et al.* 2014), which can effectively improve the mechanical properties of RAC structures. Meanwhile, the authors had systematically researched the seismic performance of steel reinforced recycled concrete (SRRC) columns in the literatures (Ma *et al.* 2013, Ma *et al.* 2015). The results indicate that SRRC

\*Corresponding author, Associate Professor  
E-mail: mahuiwell@163.com

columns have the advantages of high bearing capacity and good mechanical performance under earthquake. However, the construction operation process of the columns is relatively complicated because it needs to be reinforced with rebar skeleton and profile steel. In addition, the RAC filled steel tube columns have the characteristic of high bearing capacity, good ductility and relatively simple construction process. In view of this, a new composite structural member named SRRC filled square steel tube column was put forward in this paper. It is mainly composed of square steel tube, profile steel and core RAC, which can be regarded as a combination of SRRC columns and RAC filled steel tubes columns. Generally, profile steel is commonly set in the inside of columns and the outside steel tube can effectively provide constraint to profile steel and RAC. Obviously, the columns were able to overcome the complex construction shortcoming of SRRC columns and avoid the easy buckling of RAC filled steel tubes columns suffered the large loads. Therefore, the new columns are a kind of green building component with good mechanical properties. So far, there are few studies on the mechanical behavior of the columns, especially the nonlinear finite element analysis of the axial compressive behavior of the columns.

The nonlinear finite element analysis is a kind of numerical method. There are many other numerical methods, which can be successfully applied to solve static and dynamic problems of structural elements, such as differential transform, Rayleigh-Ritz solution, differential quadrature methods and so on. Akgoz and Civalek (2012, 2013, 2016) presented that the governing equations and the related boundary conditions are derived from the variational principles. These differential equations are solved analytically for deflection, bending, buckling, and rotation responses of micro-sized beams. Akgoz and Civalek (2013) utilized the Rayleigh-Ritz solution method to obtain the critical buckling loads of the micro-columns. Mercan and Civalek (2017) reported that the harmonic differential quadrature method was used for numerical simulations. Akgoz and Civalek (2014) derived the equilibrium equations and corresponding boundary conditions for the buckling of microbeams with the minimum total potential energy principle.

All the above numerical methods are representative methods with good accuracy, which can solve more challenging problems. However, these numerical methods have different applicability and limitations. Comparatively, the finite element analysis method has wide universality, and there are many finite element softwares, such as ANSYS and ABAQUS. Shi *et al.* (2012) conducted a finite element parametric study to study the influences of a range of parameter on the local buckling of steel columns using ANSYS. Muthuraj *et al.* (2017) carried out the numerical investigation by conducting linear and nonlinear shell finite element analysis using ABAQUS software. Additionally, some scholars had carried out a series of nonlinear analysis on the axial compression behavior of SRRC columns and RAC filled steel tubes columns. In the literature (Li *et al.* 2014, Xu *et al.* 2017), the finite element analysis on axial bearing capacity of RAC-filled square steel tube columns

had been carried out by selecting the appropriate material constitutive relationship. The research results show that the established finite element models by ABAQUS can well reflect the axial compression performance of the above columns. In the literature (Huang *et al.* 2015), the finite element analysis of RAC-filled square steel tube columns with four different cross section forms were carried out by ABAQUS software and the calculation results are in good agreement with the experimental results. In the literature (Qi *et al.* 2018), the ABAQUS software was used to analyze the stress process of SRRC columns and the validity of the result was verified compare with the test results. Therefore, the method of finite element analysis can be used to research the axial compression performance of SRRC filled square steel tube columns.

In view of this, the nonlinear finite element analysis on the axial compressive performance of SRRC filled square steel tube columns was performed by using the ABAQUS software based on the axial compression test. The failure process, deformation, stress nephogram, axial load-strain curves and axial bearing capacity of the columns were obtained. The reasonableness of finite element model was verified by comparing with the experimental results. In addition, the design parameters such as RCA replacement percentage, RAC strength, width thickness ratio of square steel tube, profile steel ratio, profile steel strength and square steel tube strength on the axial compression behavior of columns were also analyzed in detail. On this basis, in order to make the calculation results of the nominal axial bearing capacity of columns more accurate and safer, this paper refers to the formulas in ANSI/AISC 360-10 and revises the correlation coefficient of formulas. At the same time, the nominal axial bearing capacity of the columns were calculated by using the modified the formula in ANSI/AISC 360-10 and were compared with the experimental values and the numerical results, respectively. Finally, the suitably calculation formula of the nominal axial bearing capacity of the new columns was suggested in this paper.

## 2. Experimental procedures

Thirteen SRRC filled square steel tube columns were designed and manufactured in the test. Table 1 lists the main design parameters of columns. The geometric dimension and structural form of the columns are shown in Fig.1. The section size of the specimens of SRRC filled square steel tube columns is 200 mm×200 mm. The profile steel and square steel tube, which were made of Q235 steel products, were welded in the form of straight welds for the specimens. The basic mechanical properties of profile steel and square steel tube are shown in Table 2.

In addition, RCA used in the columns was derived from the demolition waste concrete by crushing and screening. The basic physical performance of RCA adopted in the test basically meets the standard requirements of "recycled coarse aggregate for concrete" (GB/T25177-2010) in China. The ordinary Portland cement with the strength grade 42.5R was used in the RAC material for the columns. Besides, the

Table 1 Design parameters of the specimens of columns

Specimen number	RAC strength	Height of columns / $l_0$	Slenderness ratio / $\lambda$	RCA replacement percentage/ $r$	Wall thickness of square steel tube/ $t$	Width-thickness ratio of square steel tube $B/t$	Profile steel ratio $\rho_a$
SPSC1	C40	500mm	8.67	0%	2mm	100.0	5.54%
SPSC2	C40	500mm	8.67	30%	2mm	100.0	5.54%
SPSC3	C40	500mm	8.67	50%	2mm	100.0	5.54%
SPSC4	C40	500mm	8.67	70%	2mm	100.0	5.54%
SPSC5	C40	500mm	8.67	100%	2mm	100.0	5.54%
SPSC6	C40	500mm	8.67	100%	1.5mm	133.3	5.54%
SPSC7	C40	500mm	8.67	100%	3mm	66.7	5.54%
SPSC8	C40	500mm	8.67	100%	2mm	100.0	4.44%
SPSC9	C40	500mm	8.67	100%	2mm	100.0	6.36%
SPSC10	C50	500mm	8.67	100%	2mm	100.0	5.54%
SPSC11	C60	500mm	8.67	100%	2mm	100.0	5.54%
SPSC12	C40	1200mm	20.78	100%	2mm	100.0	5.54%
SPSC13	C40	1800mm	31.18	100%	2mm	100.0	5.54%

Notes:  $r$  is the percentage of RCA mass in total coarse aggregate quality,  $\rho_a$  is the ratio of section area of profile steel to total area of columns;  $\lambda$  is the slenderness ratio of columns,  $\lambda=l_0/i$ ;  $l_0$  is the calculation height of columns,  $i$  is the radius of rotation of cross section in the columns

Table 2 Mechanical properties of square steel tube and profile steel

Steel type		Yield strength $f_y$ / Mpa	Ultimate strength $f_u$ / Mpa	Elastic modulus $E_s$ / Mpa
Profile steel	Flange	315.1	420.0	$2.05 \times 10^5$
	Web	309.9	437.7	$1.99 \times 10^5$
Square steel tube		270.8	363.0	$1.94 \times 10^5$

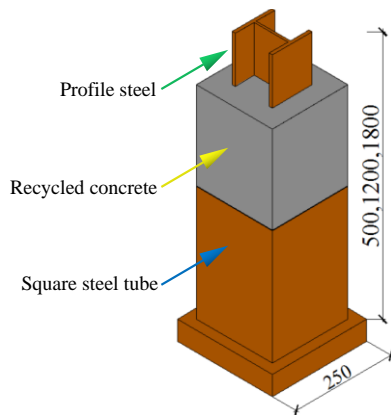


Fig. 1 Composition diagram of specimens for the columns



Fig. 2 Loading devices of axial compression tests

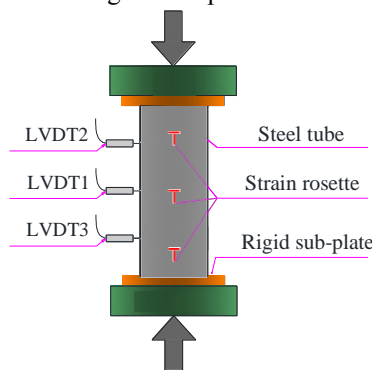


Fig. 3 Main displacement and strain measurement points of specimens

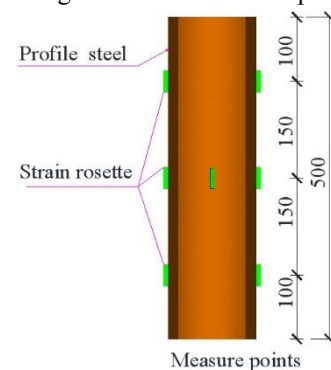


Table 3 Mix proportion and cubic compression strength of RAC material

RAC strength grade	RCA replacement percentage $r$	Water-cement ratio	Mass of the unit volume( kg/m <sup>3</sup> )							Cubic compression strength $f_{cu}$ /MPa	Elastic modulus $E_c$ /MPa
			Cement	Sand	NCA	RCA	Water	Fly ash	Water reducer		
C40	0	0.44	443	576	1171	0	195	0	0	43.6	2.750×10 <sup>4</sup>
	30%	0.44	443	576	819.5	351.3	195	0	0	43.1	2.731×10 <sup>4</sup>
	50%	0.44	443	576	585.5	585.5	195	0	0	42.5	2.726×10 <sup>4</sup>
	70%	0.44	443	576	351.3	819.7	195	0	0	41.5	2.706×10 <sup>4</sup>
	100%	0.44	443	576	0	1171	195	0	0	40.8	2.691×10 <sup>4</sup>
C50	100%	0.36	358	649	0	1138	163	94	3.5	51.3	2.884×10 <sup>4</sup>
C60	100%	0.34	380	592	0	1135	163	100	4	59.8	3.005×10 <sup>4</sup>

artificial crushed aggregate and river sand were adopted as natural coarse aggregate and fine aggregate in the mixture. In the pouring process of RAC material, the use of a small amount of water reducing agent and fly ash can effectively improve the working performance of RAC material. The mix proportions and basic mechanical properties of RAC material were shown in Table 3.

The axial compression test of the SRRC filled square steel tube columns were carried out by the 5000 kN cylinder pressure testing machine in Structural Laboratory of Xi'an University of Technology in China. The loading device of axial compression test is described in Fig. 2 and the main measuring points of profile steel and square steel tube in the columns is also shown in Fig.3.

### 3. Finite element analysis of the columns

#### 3.1 Constitutive relations of materials

In the numerical simulation, the constitutive relation is the description of the physical relationship between force and deformation in the entire loading process of material. It is also indispensable in the calculation of strength and deformation for the material. The SRRC filled square steel tube columns are composed of square steel tube, profile steel and RAC. In the whole force process, these three materials interact with each other so that they are generally in a complex stress state. In order to simulate the axial compression performance of the columns under axial loads, it is necessary to select the reasonable constitutive model of steel products and RAC. Thus, a mechanical model was also adopted to consider the interfacial bonding between steel and RAC in the columns.

##### 3.1.1 Constitutive model of steel products

The profile steel and square steel tube used in the test was Q235 low-carbon steel, which was a kind of isotropic elastic-plastic material possessing an obvious yield point. Generally, a simplified secondary plastic flow model is recommended as the stress-strain curve of steel material, which considers that the steel products directly enter into the strengthening phase after the yield of steel material and the strength of the steel in the plastic flow stage does not

change. Obviously, this kind of model not only takes into account the strengthening effect of steel material, but also reflects the mechanical characteristics of material properties for the steel products. Therefore, the model can be chosen as the constitutive model of profile steel and square steel tube in this numerical simulation. The stress-strain mathematical expression of the model for the steel products is determined by equation (1) and Fig. 4

$$\sigma_i = \begin{cases} E_s \varepsilon_i & \varepsilon_i \leq \varepsilon_y \\ f_s & \varepsilon_y < \varepsilon_i \leq \varepsilon_{st} \\ f_s + \zeta E_s (\varepsilon_i - \varepsilon_{st}) & \varepsilon_{st} < \varepsilon_i \leq \varepsilon_u \\ f_u & \varepsilon_i > \varepsilon_u \end{cases} \quad (1)$$

where,  $\sigma_i$  is the equivalent stress of steel;  $f_s$  is the yield strength of steel;  $f_u$  is the ultimate stress of steel;  $E_s$  is the elastic modulus of steel;  $E_t$  is the tangent modulus of steel;  $\zeta$  is the enhancement coefficient,  $\zeta=1/216$ ;  $\varepsilon_i$  is the equivalent strain of steel;  $\varepsilon_y$  is the yield strain of steel;  $\varepsilon_u$  is the ultimate strain of steel;  $\varepsilon_{st}=12\varepsilon_y$ ,  $\varepsilon_u=120\varepsilon_y$ . All of these values were obtained by the material test of steel products in the test.

The Poisson's ratio of the steel materials in the columns is assumed to be:

$$\nu_s = \begin{cases} 0.285 & \varepsilon_i \leq 0.8\varepsilon_y \\ 1.075(\sigma_i / f_s - 0.8) + 0.285 & 0.8\varepsilon_y < \varepsilon_i \leq \varepsilon_y \\ 0.5 & \varepsilon_i > \varepsilon_y \end{cases} \quad (2)$$

The above mentioned steel materials in the columns basically conforms to the Mises yield criteria, which is a general yield criteria especially for the metal materials. The equivalent stress of mathematical expression for the yield criteria can be shown as follow:

$$\sigma_s = \sqrt{\frac{1}{2}[(\sigma_1 - \sigma_2)^2 + (\sigma_2 - \sigma_3)^2 + (\sigma_1 - \sigma_3)^2]} \quad (3)$$

Where,  $\sigma_1$ ,  $\sigma_2$  and  $\sigma_3$  are the principal stresses of the metal materials in three directions, respectively.

The schematic diagram of the Mises yielding criterion is shown in Fig. 5. In the 3D principal stress space, the Mises yield surface is a cylindrical surface with  $\sigma_1 = \sigma_2 = \sigma_3$  as the axis. However, in the 2D plane, the Mises yield surface is

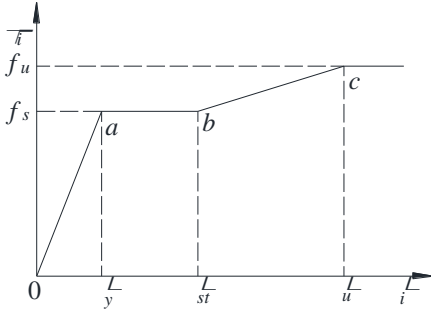


Fig.4 Stress-strain relationship of steel products

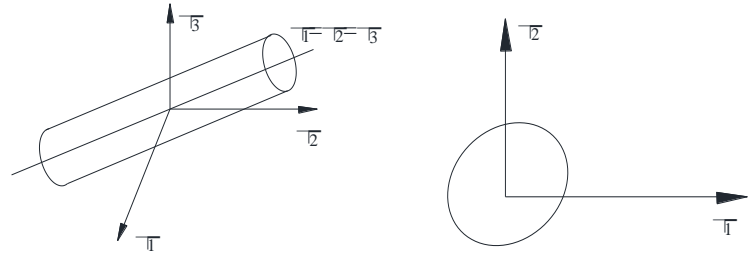


Fig.5 Schematic diagram of Mises yielding criterion

an ellipse. Any stress state inside the yield surface is elastic and any stress state outside the yield surface can cause yield. Obviously, this kind of Mises yielding criteria can be applied to the steel materials with better toughness.

### 3.1.2 Constitutive model of RAC material

The reasonable constitutive relation of RAC material is very important to the finite element analysis of the columns. RCA has the initial damage in the process of manufacture and processing compared with natural coarse aggregate, which causes that RAC has the characteristics of uneven composition and inherent micro cracks. Therefore, there is a certain difference about the mechanical properties between RAC material and ordinary concrete. In other words, the stress-strain constitutive model of ordinary concrete cannot be applied to RAC material.

In fact, some scholars have carried out many tests on the mechanical elastic modulus and compression strength of RAC material. Most of the research results show that the elastic modulus and compression strength of RAC material decrease evidently with the increase of RCA replacement percentage. The rule was also similar to that of Xiao's result (Xiao 2008). According to the stress-strain curves of RAC proposed in the literature (Xiao 2008), the mathematical equation of the constitutive relation of RAC material can be expressed by formula (4).

$$y = \begin{cases} ax + (3-2a)x^2 + (a-2)x^3 & 0 \leq x < 1 \\ \frac{x}{b(x-1)^2 + x} & x \geq 1 \end{cases} \quad (4)$$

Where  $x = \varepsilon/\varepsilon_0$ ,  $y = \sigma/f_c$ ,  $\varepsilon_0$  is the peak strain of RAC material;  $\varepsilon_0 = \{0.00076 + [(0.626f_c - 4.33) \times 10^{-7}]^{0.5}\} (1-r/B(r))$ ;  $B(r) = 65.715r^2 - 109.43r + 48.989$ ;  $f_c$  is the axial compression strength of RAC;  $f_c = 0.79 f_{cu}$ ,  $f_{cu}$  is the cubic compression strength of RAC. The values of basic mechanical properties of RAC material are shown in Table 4. Additionally, the mathematical expressions of  $a$  and  $b$  in formula (5) and formula (6) can be expressed as follows

$$a = 2.2 \times (0.718r^2 - 1.231r + 0.975) \quad (5)$$

$$b = 0.8 \times (7.6483r + 1.142) \quad (6)$$

The parameter  $a$  is the tangent slope of stress-strain curves, which reflects the initial elastic modulus of RAC. The smaller the values of  $a$  is, the greater the brittleness of

Table 4 Basic mechanical properties of RAC material

RAC strength grade	RCA replacement percentage /r	Cubic compression strength /Mpa	Axial compression strength/Mpa	Peak strain/ $\varepsilon$
C40	0%	43.6	34.4	0.002073
C40	30%	43.1	34.0	0.002062
C40	50%	42.5	33.6	0.002051
C40	70%	41.5	32.8	0.002031
C40	100%	40.8	32.2	0.002018
C50	100%	51.3	40.5	0.002210
C60	100%	59.5	47.2	0.002348

 Table 5 Values of parameters  $a$  and  $b$  for different RCA replacement percentages

RCA replacement percentage /r	0	30%	50%	70%	100%
$a$	2.2	1.32	1.26	1.15	1.04
$b$	0.8	3.3	3.96	4.31	7.5

RAC material is. The parameter  $b$  is related to the area of the descending section of the curves. The larger the value of  $b$  is, the smaller the area of the descending section of the curves is and the worse the ductile deformation of RAC is. Table 5 shows the values of  $a$  and  $b$  for different RCA replacement percentage in the test.

Considering the restraining effect of square steel tube on the RAC material, this paper refers to the constitutive relation proposed by Han (2008) and corrects the value of parameter  $b$  in the formula (4). The correction coefficient  $\eta$  expression can be as follows:

$$\eta = \frac{f_c^{0.1}}{1.2\sqrt{1+\xi}} \quad (7)$$

$$\xi = \frac{A_s f_y}{A_c f_{ck}} \quad (8)$$

Where  $f_c$  is the uniaxial compressive strength of the RAC,  $\xi$  is the constraining coefficient, and  $f_{ck}$  is the standard value of axial compression strength of the RAC.

In the finite element analysis, the damage characteristics of RAC materials need to be considered. In fact, the plastic damage model of concrete material provided by ABAQUS

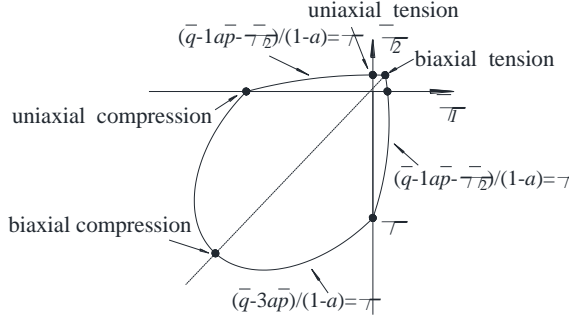


Fig.6 Yield surface in the plane stress state of RAC

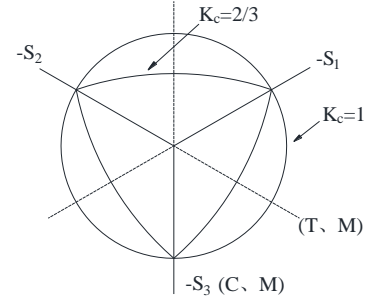


Fig.7 Yield surface in the partial stress state of RAC

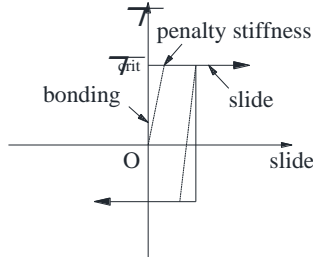


Fig.8 Interfacial shear stress and slip

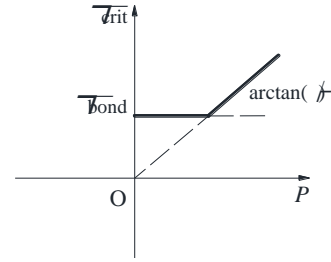


Fig.9 Interfacial critical shear stress

compression strength to uniaxial compression strength, but software not only takes into account the ratio of biaxial also considers the different performance between the compression and tensile of concrete material and the effect of biaxial compression on strength improvement. This model uses the irrelevant flow law and expansion angle can be specified as the actual dilation angle, which is more conducive to reflect the actual situation of the test. In this paper, due to lack of plastic damage model of RAC material and easy to calculate, the RAC model in this paper can be adopted the plastic damage model of ordinary concrete. The main parameters of the plastic damage model can be as follows: the dilation angle  $\psi = 35^\circ$ , the flow offset  $\varepsilon=0.1$ , the ultimate strength ratio of the biaxial compression to the uniaxial compression  $f_{bo}/f_{co}=1.16$ , the invariant stress ratio  $K_c=2/3$ , the viscosity parameter  $\mu=0.0005$ . The model considers that the failure type of RAC material is divided

into the tensile cracking and compression crushing, and its yield and failure surfaces of RAC material are controlled by the equivalent stress and compression plastic strain. It is important that two damage variables namely the tension and compression are used to describe the stiffness degradation of RAC material caused by the damage of RAC when it enters the stress-strain curve softening stage.

In this analysis, the meridian surface ( $p, q$ ) and partial plane ( $q, \theta$ ) were used to represent the yield function and plastic potential function of RAC material, which was the key factor affecting the performance of RAC. The criteria for yielding conditions are as follows

$$\sigma_1 \leq 0: f = q - 3ap + \gamma\sigma_1 - (1-\alpha)\sigma_{ci} = 0 \quad (9)$$

$$\sigma_1 > 0: f = q - 3ap + \beta\sigma_1 - (1-\alpha)\sigma_{ci} = 0 \quad (10)$$

In addition, Fig.6 and Fig.7 shows the plane and partial plane stress yield surface of plastic damage model for RAC material in the numerical model.

### 3.2 Establishment of finite element model for the columns

In this paper, two rigid end plates were used at the top and bottom of column in the finite element model, ensuring the same axial deformation among profile steel, RAC and square steel tube in the columns. When the steel and RAC entered the nonlinear phase, their stress need to be redistributed due to the plane cross-section assumption and uneven stress distribution of each material. In order to get the relatively stable load-strain curves of columns, the displacement control method was adopted in this finite element calculation. During the loading process, a key point was created at the top of the shot columns and the vertical displacement load applied to this key point for preventing the local damage of the top of columns. Moreover, a fixed hinge constraint can be applied to the lower end plate of column during the simulation by creating a coupling point transferring loads on the end plate of columns.

On the other hand, the interaction among the square steel tube, profile steel and RAC material includes the contact in the normal direction and the bond slip in the tangential direction. In addition, the normal contact adopted the hard contact in the numerical analysis. It means that there is no interaction force between the surfaces and allowed separation after contact. The bond slip in the tangential direction was established by a Coulomb friction model, as shown in Fig. 8. Once the shear stress of the interface exceeded the critical value  $\tau_{crit}$ , the relative sliding occurred between the interfaces. During the sliding process, the shear stress of the interface maintains the critical value  $\tau_{crit}$ . Fig. 9 shows the relationship between the critical shear stress  $\tau_{crit}$  and the interface normal pressure  $p$ . The mathematical expressions of bond slip are as follows

$$\tau_{crit} = \mu \cdot p \geq \tau_{bond} \quad (11)$$

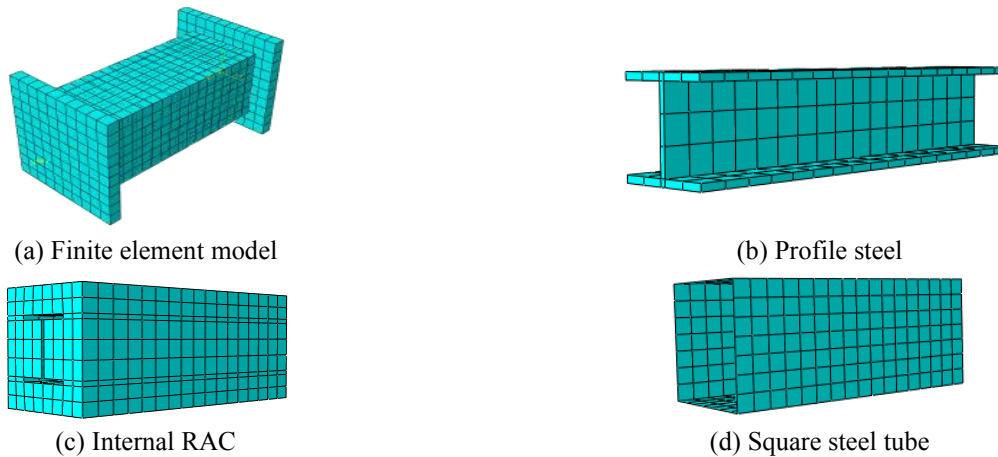


Fig.10 Mesh division of the typical columns

Where,  $\tau$  is the average interfacial adhesion bond;  $\mu$  is the friction coefficient and the friction coefficient of steel and ordinary concrete is between 0.2 and 0.6 (Balaty. P 1990). Combined with the properties of RAC used in the test and literature (Cai et al 2015), the friction coefficient can be taken as 0.25 by the trial calculation.

Taking into account the accuracy and convergence of calculation results, the square steel tube was simulated by four-node conventional shell element (SR4). The shear deformation can occur in the thickness direction of the element and the solution method follows the thick shell theory or the thin shell theory along with the change of shell thickness. The Simpson integral of nine integral points was used in the shell element thickness direction, so as to ensure the accuracy of calculation. In addition, the profile steel, end plates and RAC in the columns were modeled by 3D eight-node solid elements with reduced integration (C3D8R). The element can be used to simulate the analysis of large mesh buckling and large strain. The model grid adopts the structured meshing technique; namely, when the calculation process is non-convergence, it will re-adjust the mesh density to improve the convergence. The meshing of columns was shown in Fig.10.

#### 4. Nonlinear analysis of the columns

##### 4.1 Failure process

Using the above finite element model, the nonlinear analyses of SRRC filled square steel tube columns under axial compression loads were carried out by the finite element software of ABAQUS. Meanwhile, the deformation characteristic and stress nephogram of the columns can be obtained by finite element calculation. The columns had similar deformation characteristics and failure processes, so taking SPSC-5 as an example to illustrate the failure characteristic of columns. Fig.11 describes the comparison between the calculation and test deformation for typical SPSC 5 column. Fig.11 presents that the deformation calculated by finite element analysis is similar to the experimental deformation. Obviously, the upper part and middle part of short column occurred obvious bulging

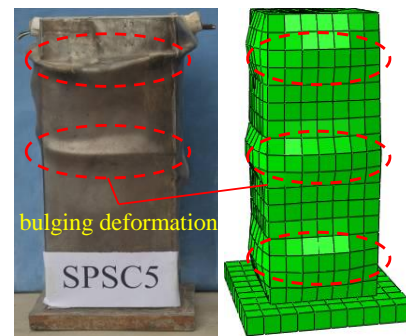


Fig. 11 Comparison between the calculation and test deformation for typical SPSC 5 specimen

deformation. Additionally, the symmetric boundary constrain were adopted on the upper and lower ends of columns in the numerical model, which leded that the columns had a symmetrical deformation characteristic under axial loads. In general, the results of finite element analysis preferably reflected the deformation characteristics of short columns more correctly.

Observing the axial compressive deformation and stress nephogram of columns shown in Fig.12-Fig.15, the following findings can be described. In the early stage of loading, the short column was in the elastic stage and the displacement increased linearly with the increase of loads. Meanwhile, there was no visible axial deformation in the columns. With the increase of axial loads, the stress in each component of columns increased continuously, especially the stress in the middle of square steel tube and profile steel increased rapidly. When the loads reached to approximately 80% of peak load ( $P_{max}$ ), the axial strain and deformation of profile steel were larger than that of square steel tube, which means that the profile steel first reached the state of yield. At that time, the cracking of internal RAC in the column increased rapidly with the increase of axial loads. Compared with the stress nephogram between the central part and end part of columns, it can be concluded that the corner of square steel tube had a strong constraint effect on RAC material, as shown in Fig.15. At this stage, the corner restraint stress of RAC material reached about 24Mpa, the overall stiffness of short columns decreased and began to enter the elastic-plastic stage. When the loads increased to

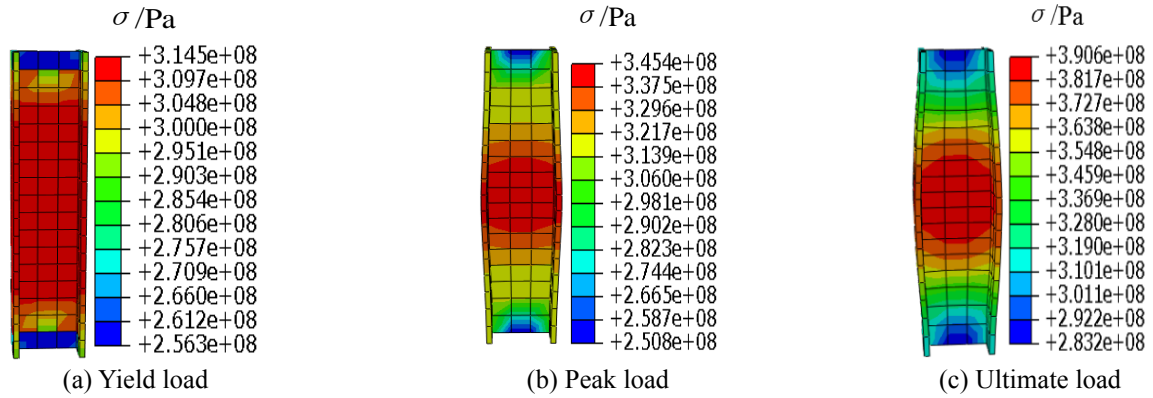


Fig.12 Stress nephogram of the main stages of profile steel in SPSC 5 specimen

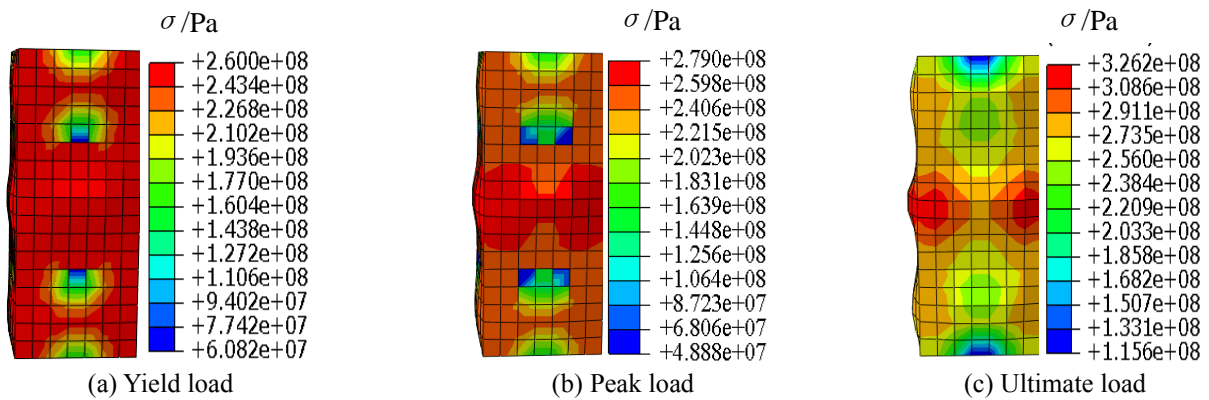


Fig.13 Stress nephogram of the main stages of square steel tube in SPSC 5 specimen

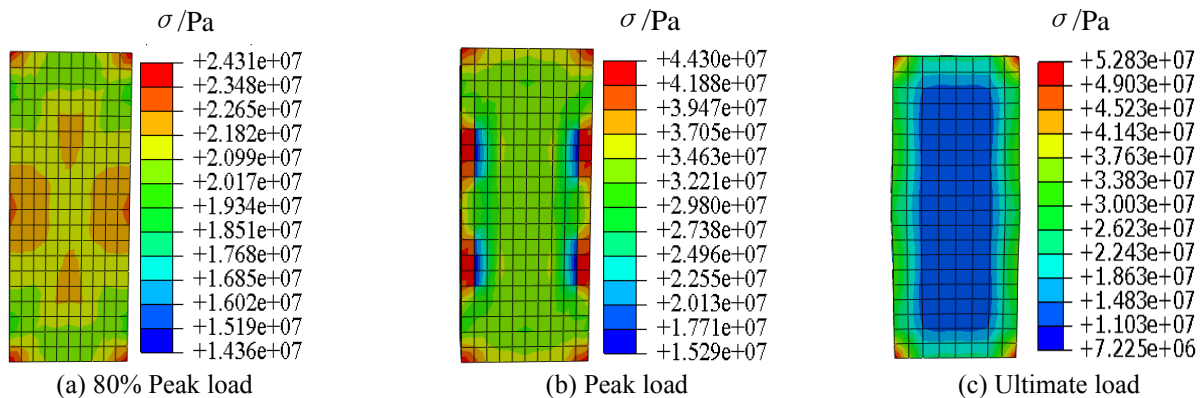


Fig.14 Stress nephogram of the main stages of the internal RAC in SPSC 5 specimen

about 90% of peak loads, the square steel tube yielded gradually and the bulging deformation in the middle part of columns was obvious. Additionally, the upper and lower ends of short columns also appeared slightly bulging. When the axial loads increased to peak loads, the middle of columns produced a significant bulging and the square steel tube at both ends of columns also produced local bulging. From the cross-section stress diagram of RAC, it can be concluded that the constraint area of profile steel to RAC was approximately circular and the restraining effect of square steel tube on the corner RAC was strengthened. When the stress of RAC in the corners of column was approximately 44Mpa, which meant the compressive strength of RAC had been exceeded its design strength. It indicates that the interior RAC in the short columns had been partially crushed. After peak loads, the axial bearing capacity of columns began to decline gradually. When the

loads drops to approximately 90% of peak loads, the axial bearing capacity of columns remained basically stable, which shows that this kind of columns possessed good deformation ability.

#### 4.2 Axial Load-strain curves

Fig.16 shows the comparison between the load-strain calculated curves and experimental curves of the columns under axial loads. Based on Fig. 16, the calculated curves of load-strain of the columns agree well with the experimental curves, which show that the established finite element model in this paper can well reflect the whole process of axial compression behavior of columns. In the early stage of loading, the columns were in the elastic stage and the strain increased linearly with increase of the loads. Significantly,

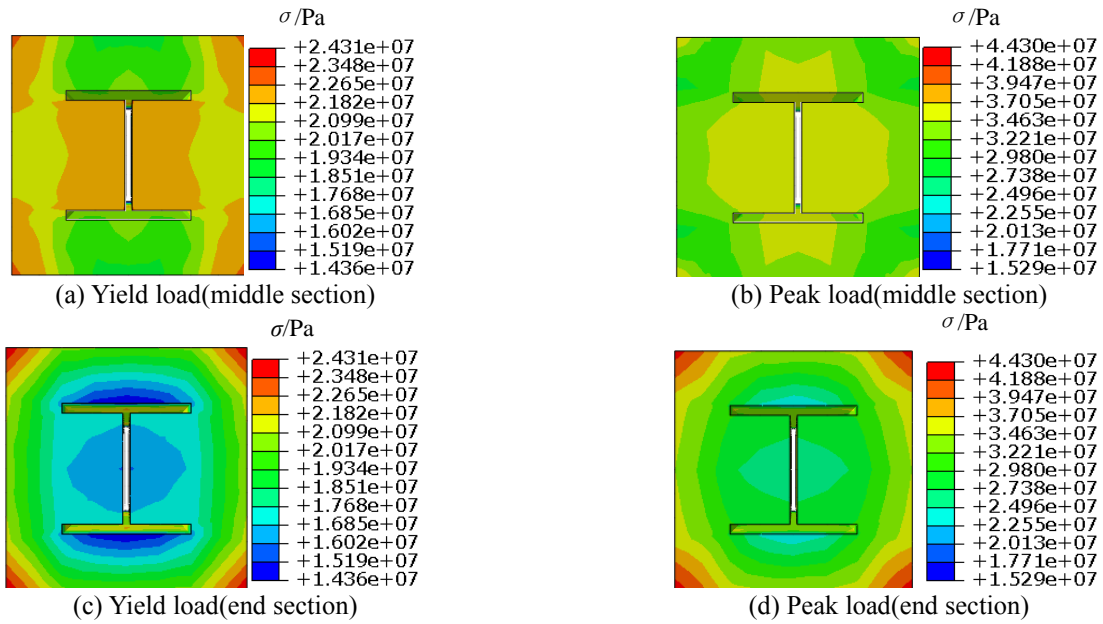
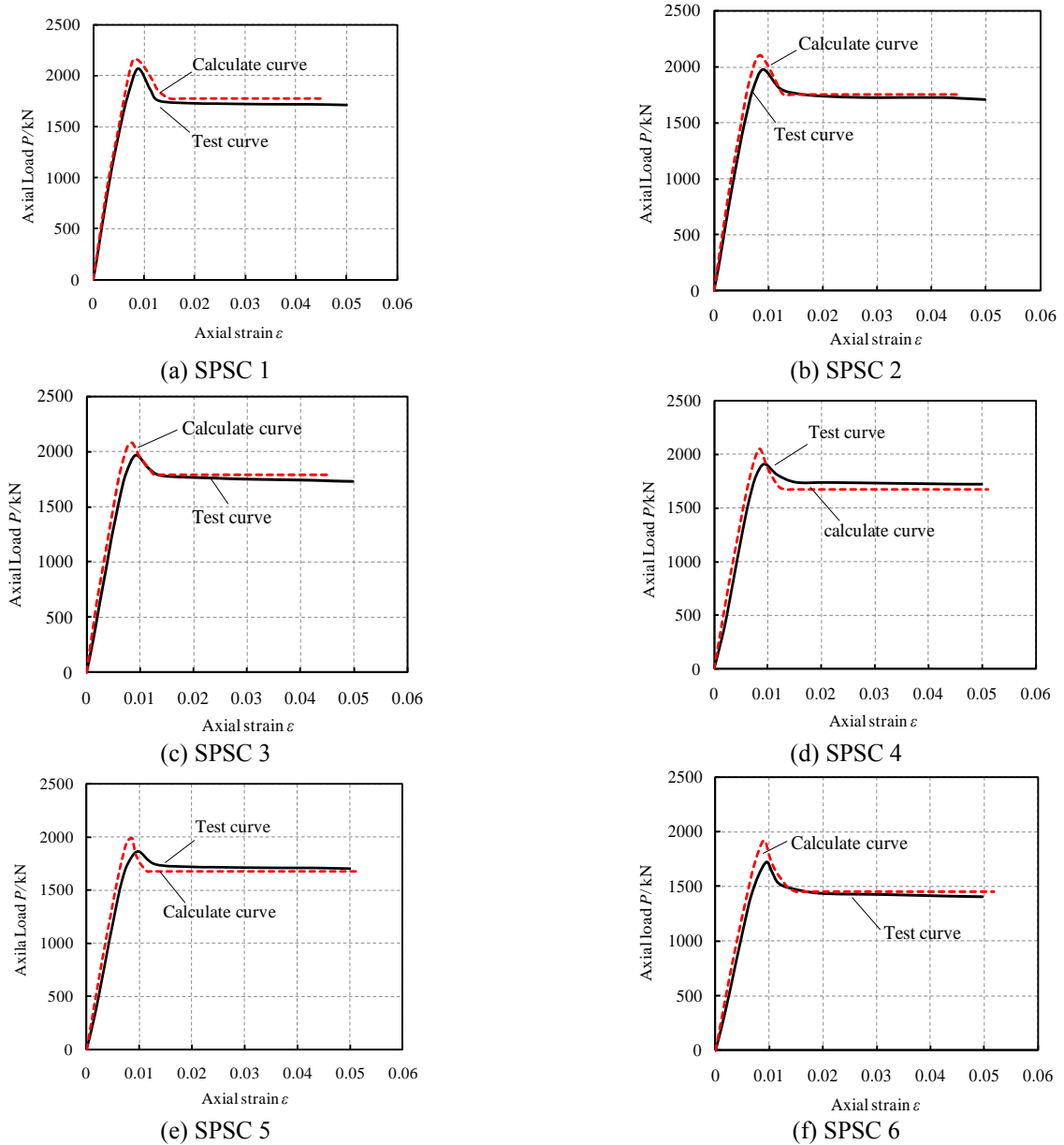


Fig.15 Stress nephogram of the main stages of internal RAC in the typical section of SPSC 5 specimen



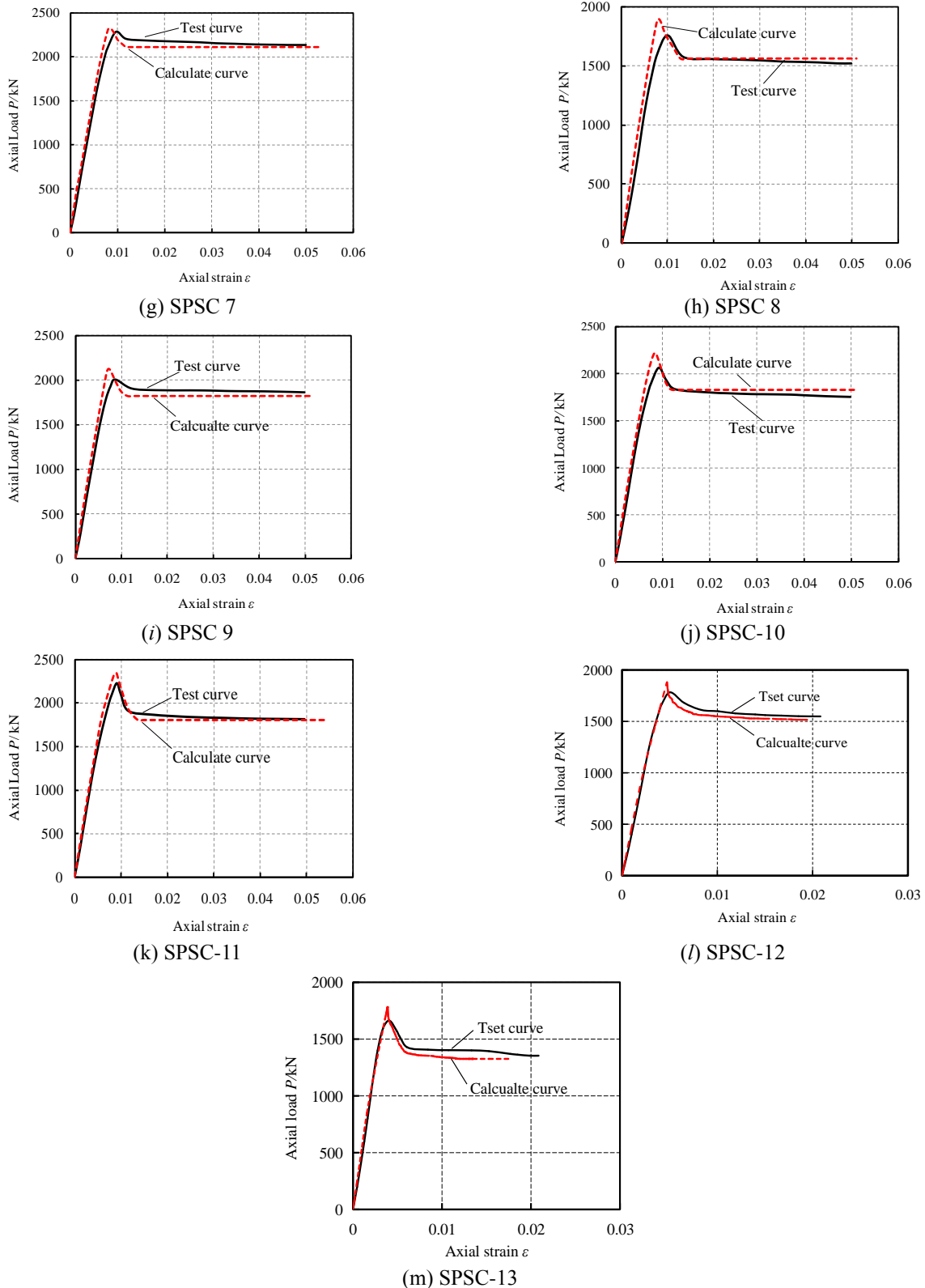


Fig.16 Comparison between the load-strain calculation curves and test curves of columns

the stiffness degradation of the column was very small. Afterwards, with the increase of axial loads, the stiffness degradation of the columns was aggravated and the columns had gradually entered into the elastic-plastic stage. Meanwhile, the load-strain curves of the column showed an obviously non-linear growth. After peak loads, the

descending section of load-strain curves of columns was relatively gentler, which indicates that the axial bearing capacity of the columns decreased slowly and it has good ductility. Generally speaking, the SRRC filled square steel tube short column has the advantages of high stiffness and high axial compression capacity.

Table 6 Comparison between the calculation values and test values of axial bearing capacity of column

Specimen number	Calculation values $N_t$ /kN	Experimental values $N_e$ /kN	Relative error %	$N_t/N_e$
SPSC1	1956.5	2067.4	5.67	0.95
SPSC2	1893.9	1981.8	4.64	0.96
SPSC3	1843.8	1966.2	6.64	0.94
SPSC4	1781.6	1911.1	7.27	0.93
SPSC5	1716.1	1862	8.5	0.92
SPSC6	1619.3	1719.6	6.19	0.94
SPSC7	1908.0	2285.2	19.77	0.83
SPSC8	1647.3	1758.3	6.74	0.94
SPSC9	1767.21	2009.4	13.7	0.88
SPSC10	2046.2	2063.3	0.84	0.99
SPSC11	2313.1	2229.9	3.6	1.04
SPSC12	1768.7	1782.7	0.79	0.99
SPSC13	1716.4	1663.4	3.09	1.03

#### 4.3 Comparison of axial bearing capacity

The comparison between the calculation values and test values of axial bearing capacity of columns are shown in Table 6. On the basis of Table 6, except the specimen of SPSC7 and SPSC9 the relative error between the calculated values and test values of axial bearing capacity of columns were less than 10%, which indicated the calculated results were in good agreement with the test results and satisfies the engineering calculation requirements. Additionally, except for SPSC11 and SPSC13 the calculation values of axial bearing capacity were lower than the test values, which were tended to be conservative. The reasons for the phenomenon and results may be as follows: 1)The defects of the constituent material itself were not fully considered in the modeling process of columns, such as the initial damage and micro cracks in the RAC material; 2)the loading process in the finite element analysis was divided into a number of analysis steps for monotonous loading, but the axial compression test was carried out under the sustained loads, which led to some errors; 3)In fact, there were some unavoidable eccentricities existing in the loading process of columns, so the columns were not fully subjected to the absolute axial compression loads in the test.

#### 4.4 Test parameters analysis

Fig.17 describes the influence of test parameters on the axial bearing capacity of the columns, which calculated by ABAQUS software. Based on Fig.17 and Table 6, it can get the following results.

From Fig.17 (a), at the initial stage of loading, the relationship between the load and strain of columns was approximately linear, which shows that the columns were in the elastic stress stage. Generally, at this stage, the RCA replacement percentage has little effect on the curves and all the specimens have similar stiffness. When the loads reached approximately 75% of peak loads, the specimens entered the elastic-plastic stage and the slope of the load-strain curves began to deviate from the initial straight line,

which means that the stiffness of columns was degraded gradually. The stiffness and axial bearing capacity of columns decreased with the increase in RCA replacement percentage. The peak load of SPSC5 column ( $r = 100\%$ ) is 7.9% lower than that of SPSC1 column ( $r=0$ ). After peak loads, the decline curve of the axial bearing capacity of columns was gentler, which indicates the short columns still have high bearing capacity and good ductility at the later stage of loading. Therefore, although this kind of columns adopted RAC material, it still has good axial compressive performance.

From Fig.17 (b), the wall thickness of square steel tube plays an important role in the stiffness and axial bearing capacity of columns. With the increase of wall thickness of square steel tube, the axial bearing capacity and stiffness of columns increased obviously. Compared with SPSC6 ( $B/t = 133.3$ ) and SPSC5 ( $B/t=100$ ), the bearing capacity of SPSC7 ( $B/t = 66.7$ ) increased by 16% and 21%, respectively. After peak loads, with the decrease of width-thickness ratio (i.e., the increase of wall thickness of square steel tube), the axial bearing capacity of columns decreased slowly, which indicates that the ductility of column were relatively good. The main reasons can be described as follows: with the increase of the wall thickness of square steel tube, it not only increases the axial bearing capacity and stiffness of columns, but also enhances the constraint effect on the internal RAC. Therefore, the reasonable design of width-thickness ratio of square steel tube has an important effect on the axial compression performance of columns.

Based on Fig.17(c), it presents that the axial bearing capacity and stiffness of the columns increased significantly with the increase of profile steel ratio. The peak load of SPSC9 column ( $\rho_a = 6.36\%$ ) is 12% higher than that of SPSC8 column ( $\rho_a = 4.44\%$ ) and increased by 7% compared with SPSC5 column ( $\rho_a = 5.54\%$ ). After peak loads, with the increase of profile steel ratio, the descent section of the load-strain curves of columns was gentler. It indicates that the ductile deformation ability of columns was enhanced with the increase of profile steel ratio. Therefore, it is beneficial to improve the bearing capacity and ductility of columns by reasonably increasing the profile steel ratio.

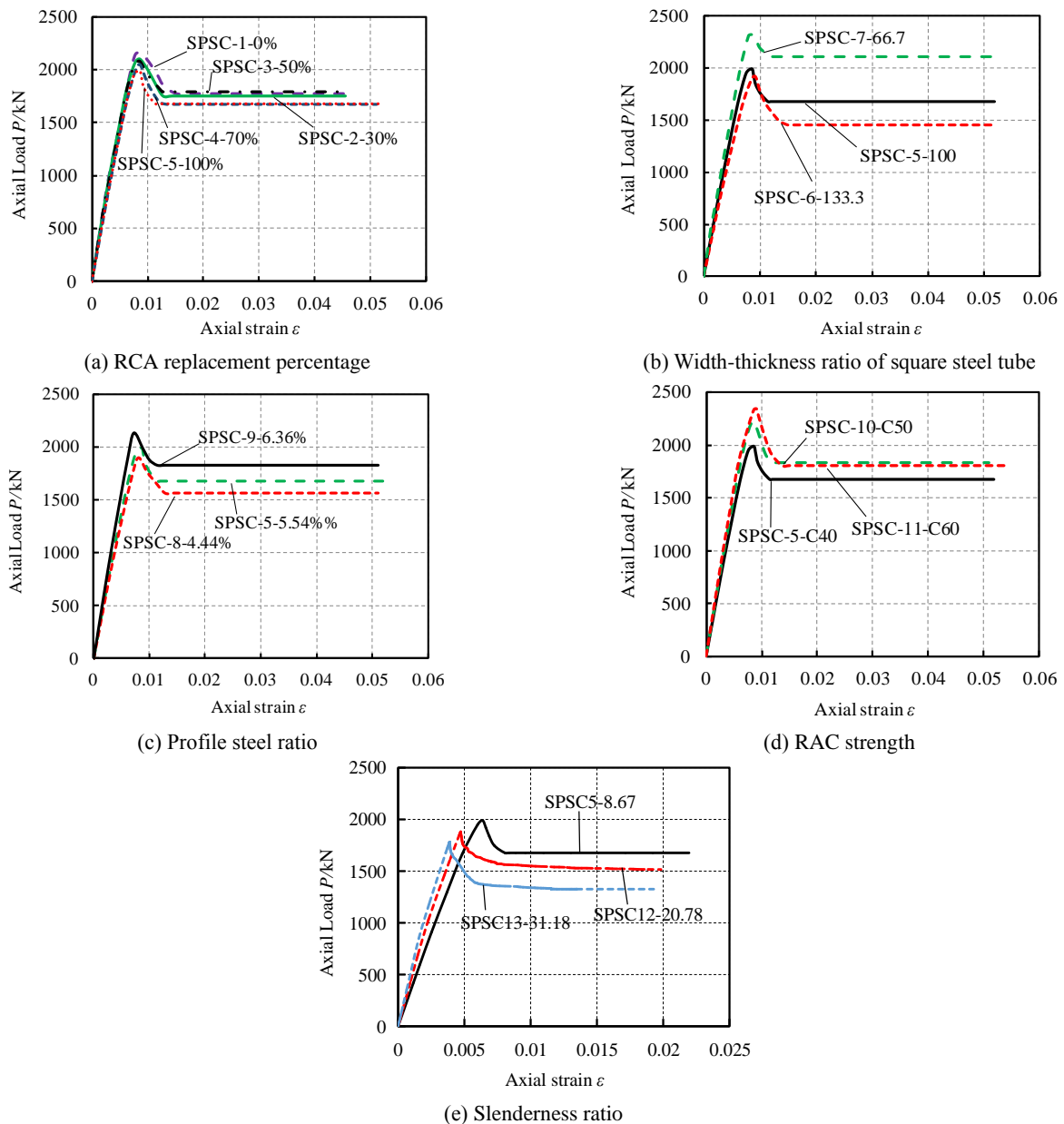
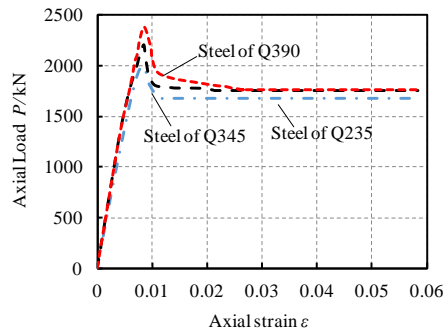


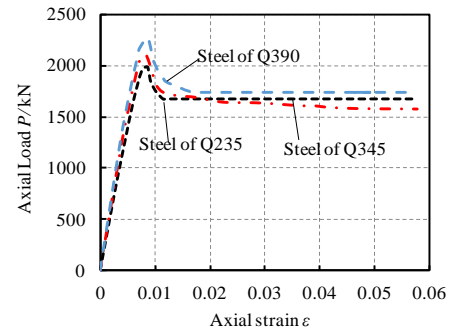
Fig.17 Influence of test parameters on the load-strain curves of columns

From Fig.17 (d), with the increase of RAC strength, the axial bearing capacity of the short columns was obviously improved. The peak load of SPSC10 column (C50) and SPSC11 column (C60) are 11.3% and 17.5% higher than that of SPSC5 column (C40), respectively. After peak loads, the axial bearing capacity of columns with a higher strength of RAC decreases faster than the columns with a lower RAC strength, which shows that the ductility of columns decreases gradually with the increase of RAC strength. The main reasons can be described as follow: with the increase of RAC strength, the brittleness of RAC material is bigger, which leads to the increasing descent rate of the axial bearing capacity of the columns. Significantly, it is necessary to adopt the appropriate RAC strength matching with the strength of square steel tube and profile steel in this kind of columns.

Fig. 17(e) depicts that the influence of the axial bearing capacity of the columns is more notable. As the slenderness ratio increases, the axial bearing capacity of the specimens gradually decreases. Compared with the SPSC-5 specimen of the short column, the axial bearing capacity of the mid-column SPSC-12 specimen is reduced by approximately 5.6%, and the long-column specimen SPSC-13 is reduced by 11.2% compared with the short-stem SPSC-5 specimen. Additionally, after the peak load, the drop rate of the specimen capacity increases as the slenderness ratio increases. It indicates that the ductility of the specimen with large slenderness ratio is poor. This is mainly because the larger the slenderness ratio, the greater the influence of the second-order effect of the column during the action of axial load, which resulting in a decrease in the axial compression performance of the long column.



(a) Strength of profile steel



(b) Strength of square steel tube

Fig. 18 Influence of finite element parameters on the load-strain curves of short columns

Table 7 Axial bearing capacity of short columns by finite element parameter analysis

Specimen number	Strength of profile steel/MPa	Strength of square steel tube /MPa	Axial bearing capacity /kN
SPSC5	Q235	Q235	1991.01
SPSC5-1	Q345	Q235	2200.03
SPSC5-2	Q390	Q235	2384.25
SPSC5-3	Q235	Q345	2109.70
SPSC5-4	Q235	Q390	2269.53

## 5. Finite element parameters analysis

According to the above analysis, the typical SPSC5 and SPSC13 specimens taken as examples, the influence law of finite element parameters on the axial compressive performance of columns was analyzed by the finite element method. And other design parameters are the same as that of SPSC5 and SPSC13 specimens respectively. Fig. 18~Fig. 19 and Table 7~8 present the results of load-strain curves and the axial bearing capacity of columns by finite element parameter analysis, respectively.

### 5.1 Finite element parameters analysis of short columns

Fig. 18 and Table 7 show that the axial bearing capacity and stiffness of columns increases gradually as the increase of the strength of profile steel and square steel tube, respectively. The bearing capacity of the specimen SPSC5-2 (strength of profile steel is Q390) was 19.7% higher than that of SPSC-5specimen (strength of profile steel is Q235) and 8.4% higher than SPSC5-1 specimen (strength of profile steel is Q345). The bearing capacity of the specimen SPSC5-4(strength of square steel tube is Q390) was 14.0% higher than that of SPSC-5 specimen (strength of square steel tube is Q235), and was 7.6% higher than specimen SPSC5-3 (strength of square steel tube is Q345). This is mainly because of the main contribution of the increased material strength and the constraint ability on the internal RAC. After the peak load, the bearing capacity of columns began to decrease gradually. Obviously, the descent rate of the axial bearing capacity of columns with a higher material

strength was clearly faster than the columns with a lower material strength. It indicates that the deformation ability of columns decreases obviously with the increase of material strength. Therefore, it is necessary to select a reasonable material strength, as far as possible eliminate the adverse effect of material strength mismatch on the axial compression behavior of columns.

### 5.2 Finite element parameters analysis of long columns

Fig. 19 (a) shows the effect of the strength of the square steel tube on the axial compressive performance of the long column. Fig. 19(a) and Table 8 indicate that as the strength of the square steel tube increases, the axial bearing capacity of the specimen gradually increases, and the bearing capacity of SPSC13-2 specimen (strength of square steel tube is Q390) is higher than that of SPSC-13 specimen (strength of square steel tube is Q235) increased by 13.6%, which was 7.7% higher than that of SPSC13-2 specimen (strength of square steel tube is Q345). Additionally, after the peak load, the trend of the falling curve phase of the specimen is basically the same, thereby indicating that the strength of the square steel tube has little effect on the ductility of the specimen.

It can be obtained from Fig. 19(b) and Table 8 that the axial bearing capacity of the specimen increases with the increased the strength of profile steel. The bearing capacity of SPSC13-4specimen (strength of profile steel is Q390) is higher than that of SPSC-13 specimen (strength of profile steel is Q235). The increase was 7.2%, which was 3.2% higher than SPSC13-3 specimen (strength of profile steel is Q345). After the peak load, the change trend of the load-strain curve falling phase of the specimen was similar, which indicates that the steel strength had no significant effect on the ductility of the long columns.

Fig. 19(c) and Table 3 show that the bearing capacity of SPSC13-6 specimen (RAC strength is C60) is 20.3% higher than that of SPSC-13 specimen (RAC strength is C40), and the SPSC13-5 specimen (RAC strength is C50) increased by 9.6%. It can conclude that the increased RAC strength is beneficial to improve the bearing capacity of long columns. Moreover, with the increase of the RAC strength, the faster the loads decreases after the peak load of the specimen, indicating that the increase of RAC strength will lead to the deterioration of the ductility of long columns.

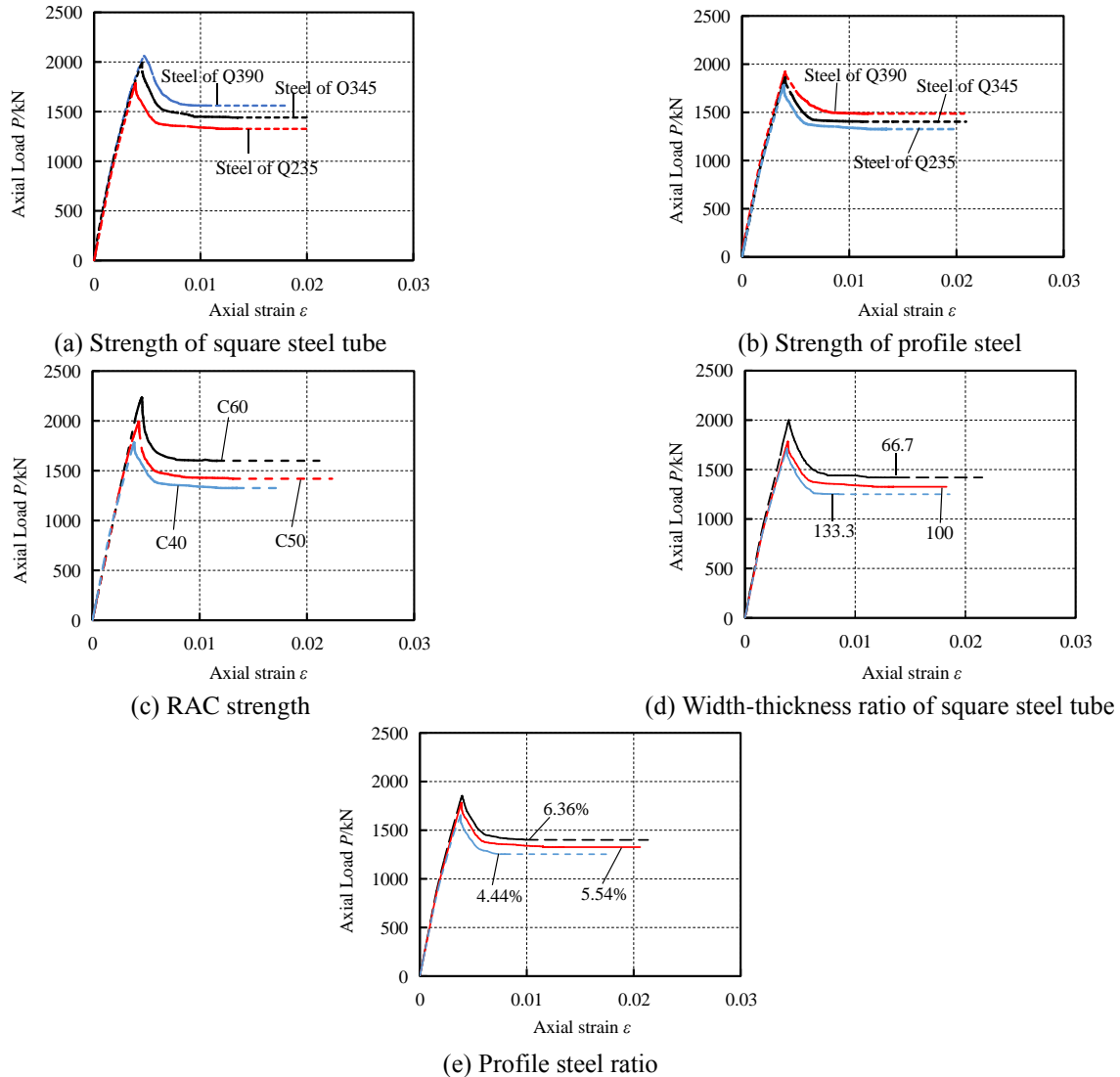


Fig. 19 Influence of finite element parameters on the load-strain curves of long columns

Fig. 19(d) shows the influence of the width-thickness ratio of the square steel tube on the axial compressive performance of the long column. According to Fig. 19(d) and Table 8, the width-thickness ratio of square steel tube has a significant influence on the axial compression performance of the long columns. With the decrease of width-thickness ratio of the square steel tube, the axial bearing capacity of the long columns increased significantly. The peak load of SPSC13 specimen (width-thickness ratio of the steel tube 66.7) was 14.7% higher than that of SPSC13-7 specimen (width-thickness ratio of the steel tube 133.3). After the peak load, the bearing capacity of the long columns begins to decrease. As the width-thickness ratio decreases, the descent segment of the long columns becomes gentler, namely, the ductility of the long columns increases with the decrease of width-thickness ratio. Therefore, the reasonable design of the width-thickness ratio of the square steel tube is very important for the axial compression performance of the long columns.

Fig. 19(e) and Table 8 depict that the axial bearing capacity of the long columns increases with the increase of

the profile steel ratio, and the maximum increase is approximately 10.8%. The profile steel mainly bears the longitudinal load in the long columns, and the raise of profile steel ratio increases the cross-sectional area of the profile steel, which effectively improves the axial bearing capacity of the long columns. After the peak load, the rate of decline of the axial bearing capacity of the long columns decreased with the increase of the profile steel ratio, which indicates that the deformation capacity of long columns was enhanced. It can be seen that the appropriate increase of the profile steel ratio can effectively improve the axial bearing capacity and ductility of the columns.

## 6. Nominal axial bearing capacity of the columns

At present, there are no related calculation formulas for SRRC filled square steel tube short columns at home and abroad. Therefore, this paper calculates the nominal axial bearing capacity of the columns on the basis of the formula in ANSI/AISC 360-10. Meanwhile, considering the

Table 8 Axial bearing capacity of long columns by finite element parameter analysis

Specimen number	Strength of square steel tube/MPa	Strength of profile steel/MPa	RAC strength/MPa	Width-thickness ratio of square steel tube	Profile steel ratio/%	Axial bearing capacity/kN
SPSC13	Q235	Q235	C40	100	5.54	1716.35
SPSC13-1	Q345	Q235	C40	100	5.54	1901.88
SPSC13-2	Q390	Q235	C40	100	5.54	2059.23
SPSC13-3	Q235	Q345	C40	100	5.54	1858.43
SPSC13-4	Q235	Q390	C40	100	5.54	1919.49
SPSC13-5	Q235	Q235	C50	100	5.54	1993.53
SPSC13-6	Q235	Q235	C60	100	5.54	2233.05
SPSC13-7	Q235	Q235	C40	133.3	5.54	1708.15
SPSC13-8	Q235	Q235	C40	66.7	5.54	2001.65
SPSC13-9	Q235	Q235	C40	100	4.44	1653.49
SPSC13-10	Q235	Q235	C40	100	6.36	1853.28

Table 9 Comparisons between calculated values and experimental values of the columns

Specimen number	calculated values/kN	Experimental values/kN	Error rate /%	Ratio of calculated values to experimental values
SPSC1	1956.5	2067.4	5.67	0.95
SPSC2	1893.9	1981.8	4.64	0.96
SPSC3	1843.8	1966.2	6.64	0.94
SPSC4	1781.6	1911.1	7.27	0.93
SPSC5	1716.1	1862	8.5	0.92
SPSC6	1619.3	1719.6	6.19	0.94
SPSC7	1908.0	2285.2	19.77	0.83
SPSC8	1647.3	1758.3	6.74	0.94
SPSC9	1767.21	2009.4	13.7	0.88
SPSC10	2046.2	2063.3	0.84	0.99
SPSC11	2313.1	2229.9	3.6	1.04
SPSC12	1768.7	1782.7	0.79	0.99
SPSC13	1716.4	1663.4	3.09	1.03
Average value( $\mu$ )			6.73	0.95

congenital defects of RAC and making the calculation results safer, this paper adds a correction factor to the formula in the ANSI/AISC 360-10. The formulas for the calculating the nominal axial bearing capacity of these columns are as follows

$$P_{no} = F_y A_s + C_1 f_c' \left( A_c + A_t \frac{E_t}{E_c} \right) \quad (12)$$

$$P_e = \pi^2 (EI_{eff}) / (KL)^2 \quad (13)$$

$$EI_{eff} = E_s I_s + E_t I_t + C_3 E_c I_c \quad (14)$$

$$C_2 = 0.6 + 2 \left( \frac{A_s}{A_c + A_s} \right) \leq 0.9 \quad (15)$$

$$P_n = P_{no} \left[ 0.658 \frac{P_{no}}{P_e} \right] \quad (16)$$

$$\frac{P_{no}}{P_e} < 2.25$$

Where  $P_{no}$  is the design values of axial bearing capacity of columns;  $F_y$  is the yield strength of steel;  $A_s$  is the cross sectional area of square steel tube;  $C_1$  is the coefficient of correction and its value is 0.85;  $f_c'$  is the compression strength of RAC,  $f_c' = 0.79 f_{cu}$ , and  $f_{cu}$  is the cubic compression strength of RAC;  $A_c$  is the cross section area of RAC;  $A_t$  is the section area of the section steel;  $E_s$ ,  $E_t$ ,  $E_c$  are the elastic modulus of square steel tube, profile steel and RAC, respectively;  $P_e$  is the elastic critical tensile stress;  $EI_{eff}$  is the equivalent stiffness of columns;  $C_2$  is the coefficient When  $C_2 \geq 0.9$ ,  $C_2 = 0.9$ ;  $L$  is the calculation

Table 10 Comparisons between calculated values and numerical results of the columns

Specimen number	Calculated values/kN	Numerical values/kN	Error rate/%	Ratio of calculated values to experimental values
SPSC5-1	1659.8	2200	32.54	0.75
SPSC5-2	1659.8	2384.25	43.64	0.7
SPSC5-3	1832.7	2109.7	15.12	0.87
SPSC5-4	1903.3	2269.5	19.24	0.84
SPSC13-1	1821.3	1901.9	4.43	0.96
SPSC13-2	1884.6	2059.2	9.27	0.92
SPSC13-3	1716.4	1858.4	8.28	0.92
SPSC13-4	1716.4	1919.5	11.84	0.89
SPSC13-5	1897.1	1993.5	5.08	0.95
SPSC13-6	2175.1	2233.1	2.67	0.97
SPSC13-7	1539.7	1708.2	10.94	0.9
SPSC13-8	1827.1	2001.7	9.56	0.91
SPSC13-9	1571.75	1653.5	5.2	0.95
SPSC13-10	1685.39	1853.3	9.96	0.91
Average value( $\mu$ )			13.41	0.89

length of columns;  $K$  is the coefficient of calculation length;  $I_s$ ,  $I_t$  and  $I_c$  are the moment of inertia of square steel tube section, moment of inertia of section steel section and moment of inertia of RAC section, respectively;  $P_n$  is the axial bearing capacity.

This paper considers the adverse influence of recycled coarse aggregate and makes the calculation result safe. On the basis of ANSI / AISC 360-10, the correction factor  $\alpha$  is added to Formula (12). It can be as follows

$$P_{no} = F_y A_s + \alpha C_1 f_c' \left( A_c + A_t \frac{E_t}{E_c} \right) \quad (17)$$

Where  $\alpha = 0.9$  for 100% RAC, and  $\alpha = 1.0$  for normal aggregate concrete. According to the RCA replacement percentage, the linear interpolation between 0.9 and 1.0 is permitted.

Table 9 shows the calculated values of the nominal axial bearing capacity of the experimental specimens based on the modified ANSI/AISC 360-10. Additionally, in order to verify the validity of the amendment of ANSI/AISC 360-10, Table 10 shows the calculated results on the axial bearing capacity for the numerical simulation samples by the modified calculation formulas. Through comparing the calculated values with the experimental values, the deviation of the experimental sample group is small. On the whole, the deviation of the finite element simulation group is larger than that of the experimental group, but the deviation of calculation is relatively smaller. Moreover, the calculated values are conservative. This is mainly because the superposition theory was adopted in this specification, which considered that steel tube, profile steel and the RAC were separately suffered from the loads and ignored the interaction among them.

## 7. Conclusions

- The nonlinear analysis on the axial compression behavior of SRRC filled square steel tube columns was carried out by the finite element software of ABAQUS. The main simulation results such as the failure process, deformation, load-strain curves and axial bearing capacity of columns agreed well with the test results, thereby verifying the rationality of finite element model.

- The maximum stress mainly concentrated in the middle part of columns, where it's buckling was visible. The stress nephogram indicate that the corner regions of square steel tube have a strong restraining effect on RAC. The failure process of the columns can be summarized as follows: the profile steel yielded before square steel tube and then the core RAC was crushed. Finally, the columns had lost its bearing capacity due to the obvious buckling.

- The analysis results show the relationship between the load and strain of columns was approximately linear at the initial stage of loading. Subsequently, the specimens entered into the elastic-plastic stage. The axial stiffness of columns began to degenerate gradually. After the peak load, the axial bearing capacity of columns decreased at the later stage of loading, but the descent rate was relatively gentler. On the whole, the deformability of the column is good.

- The axial bearing capacity of columns decreases slightly with the increase of RCA replacement percentage and slenderness ratio. With the increase of wall thickness of steel tube, profile steel ratio, strength of profile steel, strength of square steel tube and RAC strength, the axial bearing capacity of the columns was improved gradually. However, the increasing the slenderness ratio is unfavorable to the axial compression performance of the columns.

Generally speaking, this kind of columns has relatively high bearing capacity and good deformability

- According to the calculation analysis, the modified formulas of ANSI/AISC 360-10 was suggested to calculate the nominal axial bearing capacity of SRRC filled square steel tube columns, which can be taking into account the beneficial contribution of internal section steel in the columns. The deviation of calculation results is relatively small and partial to safety compared with the test results. For all that, the validity of the recommended formulas in this paper needs further verification.

## Acknowledgements

The research was financially supported by the National Natural Science Foundation of China (No.51408485), Natural Science Basic Research Plan in Shaanxi Province of China (No.2019JM-193), the Plan Projects of the Department of Housing and Urban-rural Development of Shaanxi Province (No. 2015-K129), The Scientific research project of Xi'an University of Technology (2016CX028), which is gratefully acknowledged.

## References

- Akgöz, B. and Civalek, Ö. (2012), "Analysis of micro-sized beams for various boundary conditions based on the strain gradient elasticity theory", *Arch. Appl. Mech.*, **82**(3), 423-443. <https://doi.org/10.1007/s00419-011-0565-5>.
- Akgöz, B. and Civalek, Ö. (2013), "Buckling analysis of functionally graded microbeams based on the strain gradient theory", *Acta Mech. Sin.*, **224**(9), 2185-2201. <https://doi.org/10.1007/s00707-013-0883-5>.
- Akgöz, B. and Civalek, Ö. (2013), "Buckling analysis of linearly tapered micro-columns based on strain gradient elasticity", *Struct. Eng. Mech.*, **48**(2), 195-205. <https://doi.org/10.12989/sem.2013.48.2.195>.
- Akgöz, B. and Civalek, Ö. (2014), "A new trigonometric beam model for buckling of strain gradient microbeams", *Int. J. Mech. Sci.*, **81**, 88-94. <https://doi.org/10.1016/j.ijmecsci.2014.02.013>.
- Akgöz, B. and Civalek, Ö. (2016), "Bending analysis of embedded carbon nanotubes resting on an elastic foundation using strain gradient theory", *Acta Astronaut.*, **119**, 1-12. <https://doi.org/10.1016/j.actaastro.2015.10.021>.
- ANSI/AISC 360-10. (2010), "Specification for structural steel buildings", *American Institute of Steel Construction*, Chicago, USA.
- Balaty, P. and Gjelsyilk, A. (1990), "Coefficient of friction for steel on concrete at high normal stress", *J. Mater. Civ. Eng.*, **2**(1), 46-49. [https://doi.org/10.1061/\(ASCE\)0899-1561\(1990\)2:1\(46\)](https://doi.org/10.1061/(ASCE)0899-1561(1990)2:1(46)).
- Bing, L., Qi, Z. and Shuang, M. (2014), "Finite element analysis of bearing capacity for recycle concrete filled square steel tubular stub columns under axial compression", *J. Arch. Civil Eng.*, **31**(4), 29-34.
- Cai, J., Pan, J. and Wu, Y. (2015), "Mechanical behavior of steel-reinforced concrete-filled steel tubular (SRCFST) columns under uniaxial compressive loading", *Thin-Walled Struct.*, **97**(5), 1-10. <https://doi.org/10.1016/j.tws.2015.08.028>.
- Cardoso, R., Silva, R. V., de Brito, J. and Dhir, R. (2016), "Use of recycled aggregates from construction and demolition waste in geotechnical applications: A literature review", *Waste Manage.*, **34**(49), 131-145. <https://doi.org/10.1016/j.wasman.2015.12.021>.
- Chen, H.J., Yen, T. and Chen, K.H. (2003), "Use of building rubbles as recycled aggregates", *Cem. Concr. Res.*, **17**(33), 125-132. [https://doi.org/10.1016/S0008-8846\(02\)00938-9](https://doi.org/10.1016/S0008-8846(02)00938-9).
- Chen, Z., Jinjun, X., and Ying, L. (2014), "Bond behaviors of shape steel embedded in recycled aggregate concrete and recycled aggregate concrete filled in steel tubes", *Steel Compos. Struct.*, **17**(6), 929-949. <http://dx.doi.org/10.12989/scs.2014.17.6.929>.
- Djebien, R., Hebhouh, H., Belachia, M., Berdoudi, S. and Kherraf, L. (2018), "Incorporation of marble waste as sand in formulation of self-compacting concrete", *Struct. Eng. Mech.*, **67**(1), 87-91. <https://doi.org/10.12989/sem.2018.67.1.087>.
- Goksu, C., Saribas, I., Binbir, E., Akkaya, Y. and Ilki, A. (2019), "Structural performance of recycled aggregates concrete sourced from low strength concrete", *Struct. Eng. Mech.*, **69**(1), 77-93. <https://doi.org/10.12989/sem.2019.69.1.077>.
- Han, L. H., Liu, W. and Yang, Y.F. (2008), "Behaviour of concrete-filled steel tubular stub columns subjected to axially local compression", *J. Constr. Steel Res.*, **64**(4), 377-387. <https://doi.org/10.1016/j.jcsr.2007.10.002>.
- Hawileh, R.A., Abed, F., Abu-Obeidah, A.S. and Abdalla, J.A. (2012), "Experimental investigation of inelastic buckling of built-up steel columns", *Steel Compos. Struct.*, **13**(3), 295-308. <https://doi.org/10.12989/scs.2012.13.3.295>.
- Huang, H. (2015), "Experimental research on mechanical behavior of recycled concrete-filled square steel tubular stub columns subjected to axial compression", *J. Build. Struct.*, **36**(33), 215-221.
- Jin, R. and Chen, Q. (2015), "Investigation of concrete Recycling in the U.S. construction Industry", *Procedia Eng.*, **42** (118), 894-901. <https://doi.org/10.1016/j.proeng.2015.08.528>
- Lai, Y.Y., Yeh, L.H., Chen, P.F., Sung, P.H. and Lee, Y.M. (2016), "Management and Recycling of Construction Waste in Taiwan", *Procedia Environ. Sci.*, **69**(35), 723-730. <https://doi.org/10.1016/j.proenv.2016.07.077>.
- Li, G. Q., Wang, P. and Hou, H. (2009), "Post-buckling behaviours of axially restrained steel columns in fire", *Steel Compos. Struct.*, **9**(2), 89-101. <https://doi.org/10.12989/scs.2009.9.2.089>.
- Ma, H., Xue, J., Liu, Y. and Dong, J. (2016), "Numerical analysis and horizontal bearing capacity of steel reinforced recycled concrete columns", *Steel Compos. Struct.*, **22**(4), 797-820. <https://doi.org/10.12989/scs.2016.22.4.797>.
- Ma, H., Xue, J., Liu, Y. and Zhang, X. (2015), "Cyclic loading tests and shear strength of steel reinforced recycled concrete short columns", *Eng. Struct.*, **92**(6), 55-68. <https://doi.org/10.1016/j.engstruct.2015.03.009>.
- Ma, H., Xue, J., Zhang, X., and Luo, D. (2013), "Seismic performance of steel-reinforced recycled concrete columns under low cyclic loads", *Constr. Build. Mater.*, **48**(11), 229-237. <https://doi.org/10.1016/j.conbuildmat.2013.06.019>.
- Mandal, S. and Gupta, A. (2002), "Strength and durability of recycled aggregate concrete", Australia, *Labse Symposium Melbourne*.
- Mercan, K. and Civalek, Ö. (2017), "Buckling analysis of Silicon carbide nanotubes (SiCNTs) with surface effect and nonlocal elasticity using the method of HDQ", *Compos. Pt. B-Eng.*, **114**, 34-45. <https://doi.org/10.1016/j.compositesb.2017.01.067>.
- Montero, J. and Laserna, S. (2017), "Influence of effective mixing water in recycled concrete", *Constr. Build. Mater.*, **22**(132), 343-352. <https://doi.org/10.1016/j.conbuildmat.2016.12.006>.
- Muthuraj, H., Sekar, S.K., Mahendran, M., and Deepak, O.P. (2017), "Post buckling mechanics and strength of cold-formed steel columns exhibiting Local-Distortional interaction mode failure", *Struct. Eng. Mech.*, **64**(5), 621-640. <https://doi.org/10.12989/sem.2017.64.5.621>.
- Papayianni, P. (2003), "Recycled aggregate concrete under cyclic loading", *Proceedings of the International Symposium on Role of Concrete in Sustainable Development*. University of Dundee,

Scotland, 509-518.

- Poon, C.S., Kou, S.C. and Lam, L. (2002), "Use of recycled aggregates in molded concrete bricks and blocks", *Constr. Build. Mater.*, **16**(5), 281-289. [https://doi.org/10.1016/S0950-0618\(02\)00019-3](https://doi.org/10.1016/S0950-0618(02)00019-3).
- Qi, L., Xue, J., Zhai, L., Zhao, X. and Leon, R.T. (2018), "Experimental and numerical studies on seismic performance of traditional style steel-concrete composite frame", *Compos. Struct.*, **201**(10), 514-527. <https://doi.org/10.1016/j.compstruct.2018.06.049>.
- Rosado, L.P., Vitale, P., Penteadó, C.S.G. and Arena, U. (2017), "Life cycle assessment of natural and mixed recycled aggregate production in Brazil". *J. Clean Prod.*, **12**(151), 634- 642. <https://doi.org/10.1016/j.jclepro.2017.03.068>.
- Senaratne, S., Lambronsis, G., Mirza, O., Tam, V.W.Y., Long, W.H. (2017), "Recycle concrete in structural Applications for sustainable construction Practices in Australia", *Procedia Eng.*, **23**(180), 751-758.
- Shah, A., Jan, I.U., Khan, R.U. and Qazi, E.U. (2013), "Experimental investigation on the use of recycled aggregates in producing concrete", *Struct. Eng. Mech.*, **47**(4), 545-557. <http://dx.doi.org/10.12989/sem.2013.47.4.545>.
- Shi, G., Liu, Z., Ban, H.Y., Zhang, Y., Shi, Y.J. and Wang, Y.Q. (2012), "Tests and finite element analysis on the local buckling of 420 MPa steel equal angle columns under axial compression", *Steel Compos. Struct.*, **12**(1), 31-51. <https://doi.org/10.12989/scs.2011.12.1.031>.
- Tang, Y. C., Li, L. J., Feng, W. X., Liu, F. and Zhu, M. (2018), "Study of seismic behavior of recycled aggregate concrete-filled steel tubular columns", *J. Constr. Steel. Res.*, **148**(9), 1-15. <https://doi.org/10.1016/j.jcsr.2018.04.031>.
- Thomas, C., Setién, J., Polanco, J., Alaejos, P. and De Juan, M.S (2013), "Durability of recycled aggregate concrete", *Constr. Build. Mater.*, **40**(3), 1054-1065. <https://doi.org/10.1016/j.conbuildmat.2012.11.106>.
- Xiao, J., Huang, Y., Yang, J. and Zhang, C. (2011), "Mechanical properties of confined recycled aggregate concrete under axial compression", *Constr. Build. Mater.*, **26**(1), 591-603. <https://doi.org/10.1016/j.conbuildmat.2011.06.062>.
- Xiao, J., Li, W., Fan, Y. and Huang, X. (2012), "An overview of study on recycled aggregate concrete in China (1996-2011)", *Constr. Build. Mater.*, **31**(6), 364-383. <https://doi.org/10.1016/j.conbuildmat.2011.12.074>.
- Xu, J. J., Chen, Z. P., Xue, J. Y., Chen, Y. L. and Zhang, J.T. (2017), "Simulation of seismic behavior of square recycled aggregate concrete-filled steel tubular columns", *Constr. Build. Mater.*, **149**(9), 553-566. <https://doi.org/10.1016/j.conbuildmat.2017.05.013>.
- Yang, Y. (2015), "Modeling of recycled aggregate concrete- filled steel tube (RACFST) beam-columns subjected to cyclic loading", *Steel Compos. Struct.*, **18**(1), 213-233. <https://doi.org/10.12989/scs.2015.18.1.213>.
- Yoda, K. and Shintani, A. (2014), "Building application of recycled aggregate concrete for upper-ground structural elements", *Constr. Build. Mater.*, **30**(67), 379-385. <https://doi.org/10.1016/j.conbuildmat.2013.12.096>.
- Young, B. (2005), "Local buckling and shift of effective centroid of cold-formed steel columns", *Steel Compos. Struct.*, **5**(2), 235-246. [https://doi.org/10.12989/scs.2005.5.2\\_3.235](https://doi.org/10.12989/scs.2005.5.2_3.235).
- Zhang, K. and Xiao, J. (2018), "Prediction model of carbonation depth for recycled aggregate concrete", *Cem. Concr. Compos.*, **4**(88), 86-99. <https://doi.org/10.1016/j.cemconcomp.2018.01.013>.
- Zhou, C. and Chen, Z. (2017), "Mechanical properties of recycled concrete made with different types of coarse aggregate", *Constr. Build. Mater.*, **56**(134), 497-506. <https://doi.org/10.1016/j.conbuildmat.2016.12.163>.